Dalton Transactions

Accepted Manuscript

ROYAL SOCIETY OF CHEMISTRY

www.rsc.org/dalton

Cite this: DOI: 10.1039/c0xx00000x

www.rsc.org/xxxxxx

PAPER

Magnetic relaxation versus 3D long-range ordering in $\{Dy_2Ba(\alpha\text{–fur})_8\}_n$ furoate polymer

E.Bartolomé,[a] J. Bartolomé,[b] S. Melnic,[c] D. Prodius,[c] S. Shova,[d] A. Arauzo,[e] J. Luzón,[b,f] L. Badía-Romano,[b] F. Luis,[b] and C. Turta[c]

Received (in XXX, XXX) Xth XXXXXXXXX 20XX, Accepted Xth XXXXXXXXX 20XX
DOI: 10.1039/b000000x

A novel Dy-complex formulated as $\{[Dy_2Ba(\alpha\text{-}C_4H_3OCOO)_8.(H_2O)_4].2H_2O\}_n$, $\{Dy_2Ba(\alpha\text{–fur})_8\}_n$, has been synthesized, structurally characterized, and magnetically and thermally investigated as a function of field and temperature, down to 85 mK. The α-furoate ligands consolidate 1D zig-zag chains formed by Dy_2 dimers separated by Ba ions. *Ab initio* calculations were used to determine the easy anisotropy axis direction, the gyromagnetic tensor components and the energy levels of each Dy. The heat capacity and susceptibility measurements allowed us to conclude that intradimer and interdimer interactions are ferromagnetic and of the same order, $J'/k_B \approx J''/k_B = +0.55$ K. In the absence of an applied magnetic field, the dynamic relaxation of the magnetization occurs through the fast ($\tau_I \sim 10^{-5}$ s) spin-reversal of each of the individual Dy's through a quantum tunneling (QT) process. A long-range 3D ordered state is achieved at $T_N = 0.25$ K, in which the ferromagnetically coupled zig-zag chains ($J'/k_B \approx J''/k_B = +0.528(1)$ K) running along the *c*-axis, are antiferromagnetically coupled to the adjacent chains ($J'''/k_B = -0.021(1)$ K). Critical slowing down of the QT time constant is observed when temperature approaches T_N. Under the application of a magnetic field, the QT relaxation is replaced by an Orbach process (with energy barrier $U/k_B = 68$ K and $\tau_0 \sim 10^{-9}$ s at $H = 2$ kOe) and a very slow ($\tau_s \sim 0.2$ s) relaxation process. We propose and demonstrate the proof of concept of a spintronic device, in which two different relaxation rates can be selected, and on/off switched by magnetic field biasing. The dynamical behavior of this compound is compared with another furoate to discuss the effect of competitive interactions.

I. Introduction

The discovery of magnetic slow relaxation processes in Single-Ion-Magnets SIMs [1] has boosted research in molecular complexes because of their potential interest for quantum computing as well as for studying new relaxation phenomena of basic interest [2]. Lanthanide ions with a large magnetic anisotropy arising from a large, non-zero orbital moment, are ideal for synthesizing SIMs [3]. Here in, Dy(III) ion with $S = 5/2$ and $L = 5$ coupled by spin-orbit interaction to $J = 15/2$, is especially useful and has been considered over the years as a bench for understanding the magnetism of SIMs [4].

[a] *Escola Universitària Salesiana de Sarrià (EUSS), Passeig Sant Joan Bosco 74, 08017-Barcelona, Spain. Fax: +34 932806642; Tel: +34-932805244; E-mail: ebartolome@euss.es*
[b] *Instituto de Ciencia de Materiales de Aragón, CSIC-Universidad de Zaragoza, Pedro Cerbuna 12, 50009 Zaragoza, Spain.*
[c] *Institute of Chemistry, Academy of Sciences of Moldova, Academiei 3, MD-2028,Chisinau, Republic of Moldova*
[d] *Institute of Macromolecular Chemistry "Petru Poni" Iasi, Aleea Grigore Ghica Voda, nr. 41A, 700487 Iasi, Romania*
[e] *Servicio de Medidas Físicas. Universidad de Zaragoza, Pedro Cerbuna 12, 50009 Zaragoza, Spain.*
[f] *Centro Universitario de la Defensa. Academia General Militar, Zaragoza, Spain.*

It is generally accepted that in Dy(III)-based SIMs single crystal anisotropy is the main factor driving the dynamics of the moment reversal, by means of thermal activated tunneling (TAQT), direct quantum tunneling (QT) at zero applied field, or Orbach processes at non-zero fields [5]. However, at very low temperatures, interionic magnetic interactions of dipolar or exchange origin may modify the SIM relaxation properties, or eventually, enable reaching long-range ordering [6]. Of course, to asses on these weak interactions, very low temperature experiments are required.

Our current research is focused on the study of the competition between SIM slow relaxation and ordering in furoate-based Dy(III) complexes. Furoate ligands have been earlier used in the synthesis of a variety of compounds with interesting properties [7]. In a previous work, we reported on the magnetic properties of $\{Dy(\alpha\text{–fur})_3\}_n$ [5], a complex constituted by 1D polymeric chains of Dy's coordinated by two furoic groups in bidentate-bridging mode, where the position of a capping ligand determined two distinct environmental sites, each of them presenting independent SIM behavior. At sufficiently low temperatures ($T_N = 0.669$ K) the antiferromagnetic (AF) dipolar interactions produced a transition to an equilibrium 3D ordered state.

In the present work the objective is to study in detail the competition between the SIM local fluctuations and short and long-range ordering under the condition of weak Dy-Dy interaction. A strategy to widen the interesting temperature region where the two effects compete is to weaken the Dy-Dy interactions, so as to reduce the long-range ordering temperature.

With this purpose in mind, we chose to study a new furoate polymer, $\{Dy_2Ba(\alpha\text{–fur})_8\}_n$. This compound is formed by trinuclear (Dy-Ba-Dy) clusters, coupled to adjacent molecules via furoic bridges forming zig-zag chains. Thus, the end-to-end coupling of adjacent Dy-Ba-Dy clusters results in the formation of magnetic Dy-Dy dimers.

Dinuclear lanthanide complexes represent the simplest molecular entities allowing the study of magnetic interactions [8]. H. Habib *et al.* [9] recently reviewed the most important bridging moieties that have been used in dinuclear Ln nano-magnets, including O-, N-, Cl, S-, arene- and radical-based ligands. Regarding Dy_2 dinuclear SMMs, a *pletora* of examples have been reported in the literature, showing both ferromagnetic (F) [10] and antiferromagnetic (AF) [11] intradimer coupling (see Table S1). Rinehart *et al.* have synthesized strongly-coupled dinuclear Dy-complexes using N_2^{3-} radical bridges [11b], holding the current record blocking temperature (8.3 K) for Dy-SMMs.

The anisotropic, single or polynuclear Ln entities can be connected through various spacers resulting in 1D coordination polymers with interesting magnetic properties [12, 13]. By assembling the building blocks through strong, paramagnetic spacers, ferromagnetic or ferrimagnetic chains showing Single Chain Magnet (SCM) behavior [14] can be formed [15, 16]. On the other hand, if the spacers are diamagnetic and provide weak enough interaction, each of the Ln moieties may show independent SIM / SMM slow relaxation [17]. In fact, different types of quasi-1D polymeric chains of lanthanides have been described, including linear and zig-zag [18] structures formed by periodic or aperiodic [19], similar [13] or dissimilar [20] moieties, and spin ladders [21]. In addition, a rich variety of 2D [22] and 3D [23] lanthanide complexes can be found.

In all these systems, the nature of the spacers, the intensity of the intra/supra-molecular interactions, their exchange/dipolar origin, and their ferro/antiferromagnetic character play a determinant role on the slow relaxation behavior or classical magnet behavior of the complex [4a]. Moreover, as the magnetic interaction between moieties becomes increasingly important the relaxation processes may be modified, and for magnetically dense systems long-range magnetic ordering may be achieved [24].

In this context, we report on the synthesis, structure and complete static and dynamic magnetic characterization of $\{Dy_2Ba(\alpha\text{–fur})_8\}_n$ down to very low temperatures.

The paper is structured as follows: The synthesis and structure determination of the compound are described in section III. *Ab initio* calculations, performed to assess the electronic level scheme, the ground state configuration and easy anisotropy axis of each Dy, are presented in section IV. Section V describes the theoretical framework (the alternating bond chain (ABC) model, the interchain interaction model and some original contributions) employed for the interpretation of the static experimental data. In section VI the static heat capacity and dc magnetic susceptibility data of the compound are reported and analyzed in terms of that model. In section VII the ac susceptibility results as a function of temperature, frequency and field are given. Our measurements allow us to observe SIM-like slow relaxation behavior and the transition to an equilibrium 3D ordered state, and the critical slowing down of the dominant relaxation process as the temperature approaches the long range ordering temperature. In Section VIII, we show that the relaxation properties of this complex can be used to realize a multifunctional molecular on/off field-biased double switch. Finally, in section IX the complete picture of the static and dynamical behavior of the compound is discussed in terms of the relative magnitude and nature of the intradimer, interdimer and interchain interactions. An ordered magnetic structure below the long-range ordering temperature is proposed. The dynamical behavior of $\{Dy_2Ba(\alpha\text{–fur})_8\}_n$ is compared with the previously reported furoate compound $\{Dy(\alpha\text{–fur})_3\}_n$. This comparison sheds some light into the effect of competitive interactions.

II. Experimental techniques

X-ray diffraction measurements were carried out with an Oxford-Diffraction XCALIBUR E CCD diffractometer using graphite-monochromated Mo-K_α radiation, with: λ=0.71073 Å, μ=4.279 mm^{-1}), at T=293 K. The crystals were placed 40 mm from the CCD detector. The unit cell determination and data integration were carried out using the CrysAlis package of Oxford Diffraction [25].

The magnetization, dc and ac susceptibility of powdered samples were measured, above 1.8 K, using a Quantum Design superconducting quantum interference device (SQUID) magnetometer. Ac measurements were done at an excitation field of 4 Oe, and under dc fields between 0-10 kOe, while sweeping the frequency between 90 and 13330 Hz in the ACMS option of a Quantum Design PPMS. Measurements on powdered samples were performed with and without the addition of Daphne oil, introduced to fix the grains at low temperatures. Measurements were repeated for a pellet sample to check that the oil did not affect the complex.

Heat capacity $C(T)$ under different applied fields (0-30 kOe) was measured on a powdered sample embedded in vacuum grease, using a Quantum Design PPMS. Experiments in the region of very low temperatures (85 mK<T<3 K) were carried out in an Oxford Instrument Kelvinox He^3-He^4 dilution refrigerator equipped with a custom made ac susceptibility and specific heat probe [26]. The voltage signal was converted into magnetic units (emu/mol) by scaling it with the data obtained with the SQUID susceptometer in a coincident temperature range.

III. Synthesis and Structure

The new compound $\{[Dy_2Ba(\alpha\text{-}C_4H_3OCOO)_8(H_2O)_4]\cdot 2H_2O\}_n$ was prepared following the method described in [7b] from the reaction of $Ba(C_4H_3OCOO)_2\cdot 2H_2O$ with $Dy(ClO_4)_3\cdot 6H_2O$ in mixture of $EtOH/H_2O$ in yield of 60%.

X-ray crystallography: $C_{40}H_{36}BaDy_2O_{30}$, M_r= 1459.03 g mol^{-1}, size 0.20×0.10×0.10 mm^3, monoclinic, space group $P2_1/c$, a=11.3267(10) Å, b=22.611(2) Å, c=10.5693(8) Å, β=115.899(10)°, V=2435.0(4) $Å^3$, Z=2, ρ_{calcd}=1.990 g cm^{-3}, μ(Mo$K\alpha$)=3.935 mm^{-1}, F(000)=1408, 9286 reflections in h(-13/13), k(-24/27), l(-12/13), measured in the range 6.72 ≤ Θ ≤ 26.00, completeness Θ_{max}=99.2%, 4742 independent reflections, R_{int} = 0.0276, 331 parameters, 0 restraints, $R1_{obs}$=0.0368, $wR2_{obs}$=0.0745, $R1_{all}$=0.0480, $wR2_{all}$=0.0768, GoF=1.051, largest difference peak and hole: 1.122/-1.128 e A^{-3}. CCDC – 978279.

All Dy^{3+} and Ba^{2+} ions are linked due to the bridging function of the polydentate furoic acid ligands. It results into the formation of one-dimensional coordination polymer {[$Dy_2Ba(\alpha$-

Table 1. Bond lengths (Å) for Dy and Ba atoms.

Dy1-O1	2.298(4)	Dy1-O10	2.394(4)
Dy1-O2[1]	2.342(4)	Dy1-O11[1]	2.306(3)
Dy1-O4	2.535(4)	Dy1-O1*w*	2.407(4)
Dy1-O7	2.452(3)	Dy1-O2*w*	2.359(4)
Ba1-O4	2.795(4)	Ba1-O6	2.883(4)
Ba1-O7	2.913(4)	Ba1-O9	2.862(4)
Ba1-O10	2.741(3)	Ba1-O12	2.979(4)

Symmetry code: [1] 2 – *x*, 2 - *y*, 1 - *z*

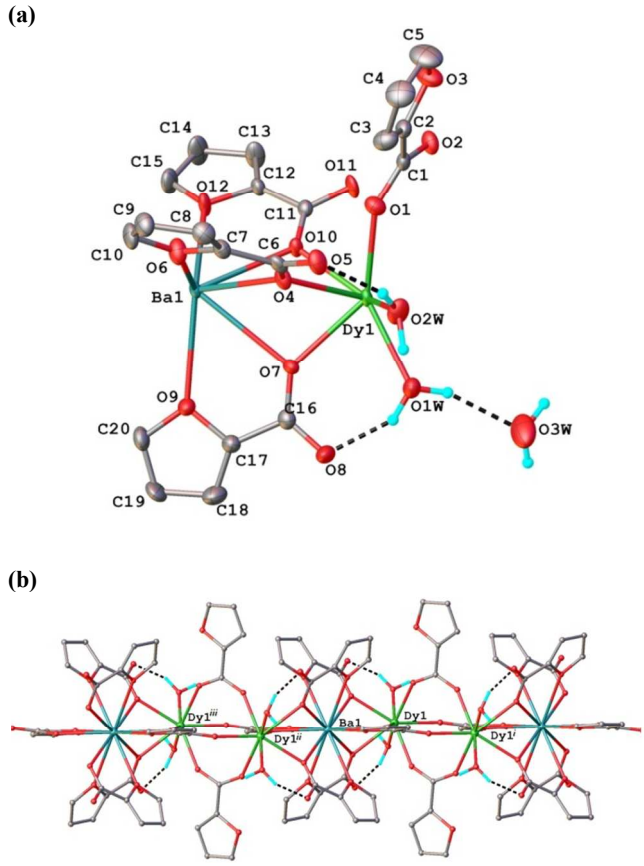

Fig. 1. (a) Asymmetric part of the unit cell along with the atomic labeling scheme; (b) A fragment of the coordination polymer $\{[Dy_2Ba(\alpha\text{-}C_4H_3OCOO)_8.(H_2O)_4]\cdot 2H_2O\}_n$, Symmetry codes: (*i*) 2 - *x*, 2 - *y*,1 – *z*; (*ii*) 2 - *x*, 2 - *y*, -*z*; (*iii*) *x*, *y*, 1 + *z*.

$C_4H_3OCOO)_8(H_2O)_4]\cdot 2H_2O\}_n$ the fragment of which along with the atom labelling scheme is depicted in Figure 1a, b. The shortest Dy···Dy and Ba···Dy separation within the infinite chain are equal to 4.471(2) Å and 4.088(2) Å, respectively. The coordination environment (O_8) of the Dy atom is provided by six carboxylic oxygen atoms and two water molecules and its coordination polyhedron can be characterized as a distorted square-antiprism (Fig. 2a). The interatomic distances in the coordination site of Dy and Ba atoms are quoted in Table 1. The coordination of Ba atom, which occupies the special position on the inversion centre can be characterized as a slightly distorted icosahedron formed by twelve oxygen atoms, originating from six furan rings and six carboxylate groups of tridentate ligands (Fig. 2b).

The coordination functions of furoate ligands in the structure are different. Each pair of Dy atoms in the chain is linked by two

Table 2. H-bonds parameters.

D-H···A	Distance, Å			Angle, deg	Symmetry code
	D-H	H···A	D···A	D-H···A	
O1w-H···O3w	0.86	2.05	2.884(6)	163.8	*x*, *y*, *z*
O1w-H···O8	0.86	1.80	2.639(7)	164.0	*x*, *y*, *z*
O3w-H···O8	0.86	2.04	2.890(7)	172.7	*x*, -*y* + 3/2, *z* + 1/2
O2w-H···O5	0.86	1.80	2.622(6)	159.4	*x*, *y*, *z*
O2w-H···O5	0.86	2.02	2.827(6)	156.3	*x* - 2, 1 + *y*, *z* - 1

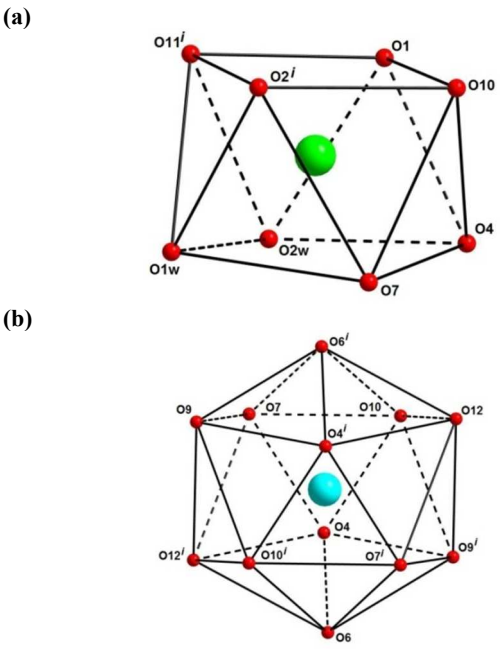

Fig. 2. (a) Coordination polyhedron on Dy atom. Symmetry code: (*i*) 2 - *x*, 2 - *y*, 1 - *z*; (b) Coordination polyhedron on Ba atom. Symmetry code: (*i*) 2 - *x*, 2 - *y*, - *z*.

carboxylate groups, which exhibit μ-O,O′ bridging function. The furan oxygen atoms of these ligands are not coordinated. Four furoic ligands exhibit tridentate-bridging function comprising one Dy and one Ba atom. The other two furoate groups act as teradentate-bridging ligands being coordinated to one Ba atom and two Dy atoms.

Polymeric 1D zig-zag chains, formed by the Dy dimers, separated by the Ba atoms are consolidated, running along the *c*-axis Fig. 3b. The packing of the coordination polymeric chains in the crystal results into the formation of a 3D supramolecular network (Fig. S1) assembled via O−H···O interchain hydrogen bonding formed by water molecules as donor and carboxylate oxygen atoms as acceptor. The geometric characteristics of the H-bonds are listed in Table 2.

IV. *Ab initio* calculations

Relativistic *ab initio* calculations were performed in order to determine the axes of the *g**-tensor of the Dy(III) ions in the $\{Dy_2Ba(\alpha\text{–fur})_8\}_n$ molecule, using the CASSCF/RASSI-SO [27] method as implemented in the MOLCAS 7.4 package [28]. This relativistic quantum-chemistry approach has proven suitable to analyse the magnetic anisotropy of lanthanide ions, and, in particular, to predict the direction of their easy axis of magnetization (EAM) [29].

Ab initio calculations were performed on a molecular cluster in which the atomic positions were extracted from the x-ray crystal structure. The cluster model includes the Dy ion, an Y(III) ion in the position of the other Dy ion of the dimer and the two closest Ba ions. The model also includes the furoic ligands and water molecules surrounding the studied Dy ion. In order to reduce the computation time without a significant loss of accuracy, the other ligands around the second Dy ion and the two Ba ions are adequately replaced by either OH- groups or water

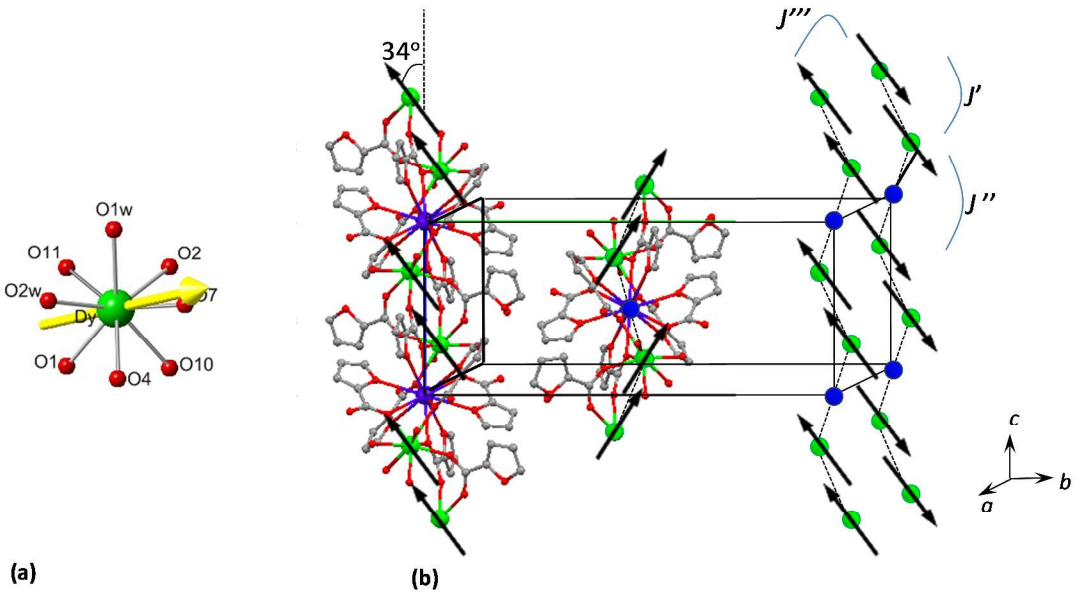

Fig. 3 (a) Calculated direction of the easy axis of magnetization; (b) Schematics showing the assembly of dimer zig-zag chains, and the definition of the intradimer (J'), interdimer (J'') and interchain (J''') coupling constants.

molecules. The replacement of the second Dy ion by an Y ion is done in order to reduce the active space. After that, the CASSCF active space consisted of the Dy 4f orbitals, containing nine electrons in seven orbitals [CASSCF(9,7)]. Preliminary studies of averaged-state CASSCF calculations including all sextets (21 roots) and all quadruplets (224 roots) revealed a low effect of the ^{6}F and ^{6}P sextets and of all quadruplets on the anisotropy of the ground state and on the energy gap between the ground and the lowest excited states of the $^6H_{15/2}$ multiplet. Therefore, in the final calculations only the ^{6}H states were considered. This allowed a larger flexibility for the basis set to describe the averaged molecular orbitals and permitted the application of the CASPT2 correction to all energy levels.

The *ab initio* calculations evidence that the Dy ground state is made of a 79% of $|J,M_J\rangle=|15/2,\pm15/2\rangle$ and a 14% $|15/2,\pm11/2\rangle$, while the rest of the doublets, including the first-excited one, contain a mixure of the different $\pm M_J$ states (Table S2). The computed energy gap between the doublet ground-state and the first excited doublet is Δ/k_B=73.4 K. For the doublet ground-state, the *ab initio* calculated gyromagnetic factors along the main single-ion anisotropy axes indicate a large uniaxial magnetic anisotropy, with g_z*=18.7, much larger than the others (g_x*=0.1, g_y*=0.3), within an effective S*=1/2 ground state description. Since the two Dy's of the trinuclear cluster building block occupy equivalent symmetry sites, their easy anisotropy axes are parallel to each other, contained within the crystallographic *bc*-plane and forming a θ=34° angle with the *c*-axis. The easy axis being almost on the *bc*-plane is not due to symmetry reasons and therefore this fact is purely accidental. The symmetry of the eight oxygen atoms surrounding each Dy ion is close to C_4, however, the EAM is not collinear with this pseudo symmetry axis, but inclined an angle of 44° with respect to it (Fig. 3a).

V. Theory: the alternating bond model

In this section we shall describe the model system used to rationalise our experimental results. The Dy-Ba-Dy trinuclear cluster molecules are arranged in zig-zag chains along the *c*-axis (see Fig. 3b), with alternating exchange constants; i.e. the system approaches the so called Alternating Bond Chain model (ABC). The interaction constant J', involving the shortest Dy-Dy distance, takes place via two furoic ligands which bind two adjacent molecules creating a magnetic Dy-Dy dimer, while the interaction constant J'' describing the coupling to the n.n. Dy in the chain, is via several Dy-O-Ba-O-Dy pathways. Each of these chains has four adjacent chains that may couple via an interchain exchange J_{ic}. The number of n.n.n and n.n.n.n. Dy atoms interacting is not evident, so, as an approximation we consider the interchain interaction to take place with four n.n.n (z'''=4) Dy atoms and an average interaction J'''. In principle $J'\neq J''$ and it is expected that $J', J''>J'''$.

Besides, as it is discussed in section IV, each Dy(III) has strong uniaxial anisotropy, with an energy separation between the ground state Kramers doublet $|S_z=\pm15/2\rangle$ to the first excited doublet of Δ/k_B=73.4 K. At low temperatures only the ground doublet is thermally occupied, so an effective S*=1/2 ground doublet, projection of the real one, may be assumed. Moreover, the adjacent Dy atoms lie in the same type of crystallographic site, therefore the spins of the two Dy in the same molecule and two adjacent molecules need to be parallel (or antiparallel) by this symmetry constraint. It can be concluded that at low temperatures the Dy-Dy couplings are of the Ising type, with the *z*-axis fixed by the anisotropy axes of the Dy ions in the chain.

Therefore, the model system is described as dimers with intradimer exchange J', interacting with adjacent dimers along the chain with J'', and interacting with adjacent chains via J'''.

The total Hamiltonian may be described as: $H=H_{ABC}+H_{ic}+H_z$. The Alternating Bond Chain Hamiltonian reads as:

$$H_{\mathrm{ABC}} = -2\sum_{i=1}^{N} J(i,i+1) S^*_{i,z} S^*_{i+1,z}, \qquad [1]$$

with $J(i, i+1)=J'$ and J'' for i= even and odd, respectively, and N extends to infinity.

The interchain interaction Hamiltonian is:

$$H_{ic} = -2J''' \sum_{\substack{i>j \\ nnn}} S^*_{i,z} S^*_{j,z}, \qquad [2]$$

and:

$$H_z = -\sum_i \mu_B g^*_z S^*_{i,z} H\cos\theta, \qquad [3]$$

is the Zeeman term for a constant magnetic field applied at an angle θ with respect to the atomic anisotropy axis.

At temperatures, $T>>J''/k_B$, one may neglect H_{ic} and, therefore, the model reduces to non-interacting ABC chains. For this model analytical expressions for the zero field susceptibility in the z direction and heat capacity have been obtained for the Ising, $S^*_z = 1/2$ model, by means of the transfer matrix method [30]. From the highest eigenvalue of the transfer matrix $\lambda_+=\lambda(x)$ with $x=1/T$ (Eq. [27] in ref. [30]) the thermodynamic functions can be calculated.

For 2 magnetic atoms per formula unit, as is our case, the susceptibility in the z-direction per mol is:

$$\chi^z_{ABC} = \frac{N_A g^{*2}_z \mu_B^2}{k_B T\left[\exp(-J'/k_B T) + \exp(-J''/k_B T)\right]}. \qquad [4]$$

For a powder, $\chi_{powder} = \chi^z_{ABC}/3$, since for the Ising model the perpendicular contribution is zero. Taking into account the demagnetization factor of our sample N_d=5.7x10^{-3} mol/emu, the measured susceptibility becomes:

$$\chi(T) = \frac{\chi^{powder}}{1 + N_d \chi^{powder}}. \qquad [5]$$

Besides, the zero field heat capacity can be obtained from the partition function in terms of $\lambda(x)$ given in [30]:

$$C/R = \frac{1}{4T^2}\left[\frac{(J'/k_B)^2}{\cosh(J'/2k_B T)} + \frac{(J''/k_B)^2}{\cosh(J''/2k_B T)}\right]. \qquad [6]$$

It is interesting to note that the expressions for the particular case of non-interacting dimers are obtained by setting $J''=0$.

For $H\neq 0$ the free energy of the ABC model is given for a field applied in the z direction (Eq. [29] in ref. [30]) as:

$$F(T) = -\frac{1}{2} k_B T \ln\lambda(x). \qquad [7]$$

Since we are dealing with the ideal Ising model, the partition function for a field applied at an angle θ with respect to the z-axis of anisotropy is obtained by substituting the field by $H_z=H\cos\theta$. Although no analytical expression can be obtained for $H\neq 0$, the heat capacity for a system of $2N_A$ magnetic atoms can be numerically calculated from the derivative:

$$C/R = \frac{1}{T^2}\frac{\lambda\lambda'' - \lambda'^2}{\lambda^2}, \qquad [8]$$

with $\lambda'(x)$ and $\lambda''(x)$ the first and second order derivatives with respect to x. In a second step, the angular averaged specific heat for the powder sample is calculated as:

$$\overline{C}_m = \frac{\int_0^{2\pi} d\varphi \int_0^{\pi} C(\theta,\varphi)\sin\theta d\theta}{\int_0^{2\pi} d\varphi \int_0^{\pi} \sin\theta d\theta}. \qquad [9]$$

The high temperature tail of the magnetic heat capacity for interacting ABC chains can also be expressed in terms of the three interactions involved, for $2N_A$ atoms:

$$C/R = \frac{1}{4}\left(J'^2 + J''^2 + z'''J'''^2\right)/(k_B T)^2. \qquad [10]$$

Although we have developed the theoretical predictions of $\chi^z(T)$ and $C(T)$ for $J'\neq J''$, in the present work we shall show below that the zero field susceptibility and heat capacity can only be fitted if $J'\approx J''$. Therefore, the ABC chain model becomes an Ising chain with homogeneous $S^*=1/2$ spins and bonds. The magnetic and thermal properties of this system at high temperatures and near T_N were theoretically studied by Navarro *et al*. [31]. These predictions will be applied to fit the data and obtain a more reliable value of the interchain constant.

The heat capacity for this Ising $S^*=1/2$ model has been studied as a function of the interaction constant ratio $r=J'''/J'$ ($J'>0$, $J''<0$), which allows describing the evolution from the single chain to the 3D case. The slope of the high temperature heat capacity per dimer mol can be expressed in terms of J' and r as:

$$C/R = aT^{-2} = \left(\frac{1}{2} + r^2\right)\left(\frac{J'}{k_B}\right)^2 / T^2. \qquad [11]$$

This expression can be derived from Eq. [10] for $J'=J''$ and $z'''=4$.

At temperatures $T\approx J'''/k_B$ the effect of the interchain interaction manifests itself by inducing a transition to 3D long range order at T_N long range ordering. The ordering temperature T_N becomes non-zero as soon as $J'''\neq 0$. It has been calculated as a function of $J'$and r [31]. Thus, by considering the high temperature heat capacity peak tail and T_N, one can estimate the J' and J''' exchange interaction parameters.

The temperature dependence of the susceptibility $\chi'(T)$ can then be theoretically calculated by using the reduced curves $\overline{\chi}_z(T,r)$ in the z direction given in [31] for different r ratios:

$$\chi^z_{chain} = \frac{N_A g^{*2}_z \mu_B^2}{2J'}\overline{\chi}(T,r). \qquad [12]$$

Then, considering that in this case $\chi^x = \chi^y = 0$, $\chi_{powder} = \chi^z_{chain}/3$, and the demagnetization correction is given by Eq. [5], the prediction for the equilibrium low temperature susceptibility is obtained, to be compared with the experimental data.

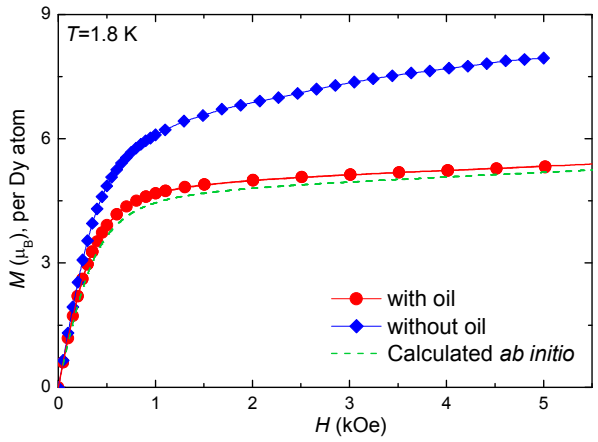

Fig. 4. Dc magnetization as a function of the applied field, $M(H)$, measured at 1.8 K, with and without oil. (Dashed line) The in-oil data are compared to the predicted curve using the *ab initio* calculated eigenfunctions and eigenvalues (S3).

VI. Dc measurements

Magnetization. Fig. 4 shows the magnetization as a function of the applied field, $M(H)$ per Dy at 1.8 K, measured for a powdered sample, with and without the addition of an oil droplet. The in-oil $M(H)$ curve is compared to the predicted curve, calculated using the canonical ensemble statistics with the eigenvalues and eigenvectors (see S3) obtained from the *ab initio* calculations described in Section IV, and considering any interionic interaction as negligible. The calculations have assumed a randomly oriented powder. The constant slope above 1 kOe is caused by the mixing of the ground state with the excited states, the so-called Van Vleck contribution. Such an excellent reproduction by the simulations shows that the *ab initio* results are very robust, on one hand, and that the interionic interactions are negligible at this temperature and field range. The van Vleck contribution has been estimated as χ_{VV}=0.01 μ_B/kOe (5.5x10^2 emu/mol).

Without the use of oil, grains are allowed to reorient under the action of the applied magnetic field. Note that they are not proportional. The magnetization at high fields is lower than the value expected for a completely oriented sample in Ising configuration, once the van Vleck contribution is subtracted, $M_{sat}^{Ising}=g_z^*S_z^*=10\mu_B$, which may be explained by the presence of spin canting (Fig. 3(b)). Indeed, assuming the *ab initio* predicted angle θ=34°, the experimental value $M_{sat}^{oil}=g_z^*S_z^*\cos\theta\approx8\mu_B$ is retrieved.

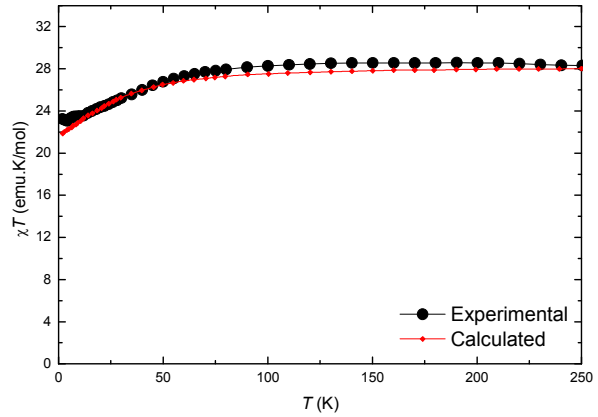

Fig. 5. The dc susceptibility-temperature product (χT) of a powdered sample in oil (●); theoretical curve calculated using the *ab initio* calculated eigenfunctions and eigenvalues (S3) (♦).

Dc susceptibility. The χT product per mol of {$Dy_2Ba(\alpha$-fur)$_8$} tends to a constant value $C=2g_J^2J(J+1)/8=28.58\mu_B^2$ above 100 K (Fig. 5). This yields an effective paramagnetic moment of μ_{eff}=10.69 μ_B, and for J=15/2, an experimental value of g_J=1.33(9), very close to the free ion limit (g_J=1.333).

As the temperature is lowered χT decreases due to the depopulation of the electronic states. Indeed, the observed decay of χT could be theoretically reproduced considering the *ab initio* calculated eigenvalues and eigenfunctions (See Table S2), assuming thermal population of the different levels, without any fitting parameters (Fig. 5).

Heat capacity. The heat capacity was measured as a function of temperature between 0.35-26 K under different applied fields in a PPMS; further measurements under zero field were carried out down to 0.2 K in a dilution refrigerator (Fig. 6a). The lattice contribution dominating the heat capacity above 4 K was fitted by

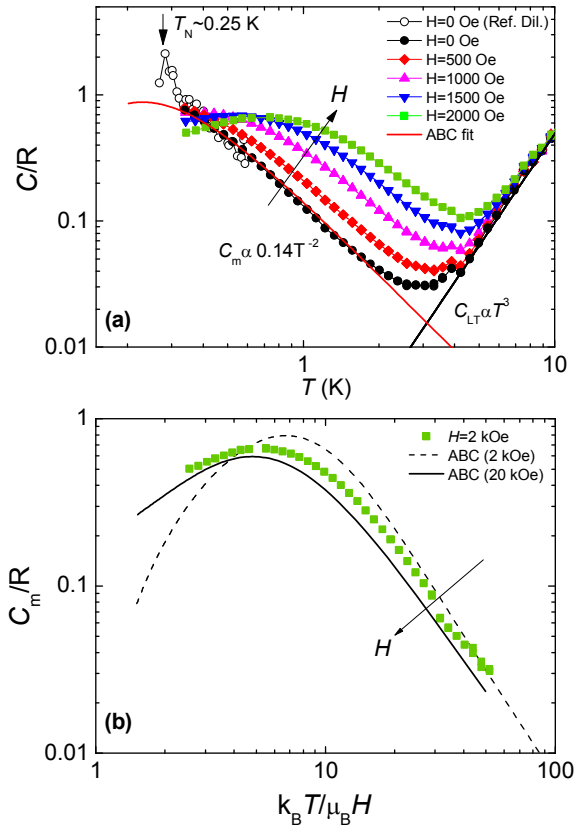

Fig. 6. (a) Heat capacity per mol as a function of temperature at different applied fields. The lattice contribution follows the dependence $C_{LT}/R=5.5x10^{-4}$ T ^{3}. The H=0 curve has been fitted with the ABC model, Eq. [6], using $J'/k_B=J''/k_B=+0.55$ K; (b) (Symbols) Magnetic contribution to the heat capacity, $C_m/R=(C-C_{LT})/R$, *vs.* the reduced parameter k_BT/μ_BH, at H=2000 Oe; (dashes) Prediction for a random orientation averaged C_m with the same J' and J'', and the *ab initio* g^* values at H=2000 Oe; (full line) Prediction for $H\rightarrow\infty$.

the Debye approximation, $C_{LT}=AT^3$, with $A/R=5.5\times10^{-4}$ K^{-3}, from which a Debye temperature of $\theta_D=359.2$ K was obtained, and the average sound velocity in the system, calculated as: $c_s=(k_B/\hbar)\theta_D(6\pi^2N/V)^{-1/3}$, where N is the number of molecules per unit cell, and V the cell volume, yielded $c_s=4.77\times10^5$ cm/s.

The zero-field heat capacity could be univocally fitted down to 0.32 K in terms of the ABC model, Eq. [6], considering ferromagnetic intradimer and interdimer interactions $J'/k_B=J''/k_B=+0.55$ K and neglecting interchain interactions. The tail of the high temperature magnetic heat capacity follows a $C_m/R=0.14T^{-2}$ dependence.

At lower temperatures, intrachain coupling becomes relevant, and enables long-range ordering. Indeed, the heat capacity exhibits a peak in the vicinity of 0.25 K; though the large data scattering prevents a more accurate determination, the ac susceptibility measurements, later shown in section VII.A, will confirm that this C_m peak is the signature of a long-range 3D ordering transition at $T_N=0.25\pm0.01$ K.

Given that the experimental data can only be fitted under the condition $J'\approx J''$, the system can be treated as an ensemble of 1D Ising chains of $S^*=1/2$ spins coupled by J', with interchain coupling J'''. Using Eq. [11], where the high temperature heat capacity tail dependence on the ratio $r=J'''/J'$ is given explicitly, and the predicted values of $T_N/J'=k(r)$, under the approximation of $z'''=4$, ($r=-0.04$, $k=0.495$), the parameters $J'=J''=+0.528(1)$ and $|J'''|/k_B=0.021(2)$ K, are obtained. We note here that the sign of the interchain constant cannot be known from the heat capacity, but its AF character will be later evidenced by ac susceptibility measurements (section VII.A).

Figure 6a also shows the data measured at several field values. In Fig. 6b the magnetic contribution to the specific heat measured at a field of $H=2000$ Oe , is depicted as a function of the adimensional parameter $T^*=k_BT/\mu_BH$, after substracting the lattice contribution. It is compared to the prediction for a randomly oriented collection of ABC chains at the same field (Eq. [8]-[9]), using the *ab initio* g^* values, with J' and J'' values obtained from the $H=0$ fit, and with the prediction at a field ($H=20$ kOe) high enough to obtain a convergent calculated curve. The experimental data fall between both predictions. It means that the powder averaging rounding effect is stronger than that predicted for an ideal Ising. The roundness of C_m at lower temperatures is better mimicked by the $C_m(H\rightarrow\infty)$, as may be expected when the applied field is much higher than any exchange effect.

VII. Dynamic magnetic properties

A. Low temperature range 85 mK<*T*<3.0 K

Zero-field. We consider below the low temperature χ' data at $f=240$ Hz as an approximation to the equilibrium susceptibility. The justification is done *a posteriori* in view of the dynamics. At sufficient low temperature (<0.6 K) the interaction between chains, J''', allows long-range ordering. A 3D long-range order transition occurs at the critical temperature $T_N=0.25\pm0.1$ K, determined from the inflection point of $\chi'(T)$ [32]. This value of T_N coincides with the temperature of the heat capacity peak, thus corroborating the determination of the long-range order transition. The value of the susceptibility maximum $\chi'_{max}(f=240$ Hz)≈96 emu/mol is lower than the ferromagnetic limit, $\chi_{limit}=1/N_d=1.75\times10^2$ emu/mol, indicating that the long-range ordering is AF.

The high temperature tail ($T>0.6$ K) of the low frequency susceptibility curve, $\chi'(T, 240$ Hz), can be fitted using the ABC model, Eq. [4], averaged over a random orientation of anisotropy axes and corrected from demagnetization effects, with the same parameters $J'/k_B=J''/k_B=+0.55$ K obtained from the heat capacity (see Fig. 7 (a)).

As explained in section V, since $J'\approx J''$, the predictions of $\chi'(T)$ close to criticality [31] for ferromagnetic Ising chains antiferromagnetically coupled, Eq. [12] instead of Eq. [4], can be applied to obtain more accurate values of the

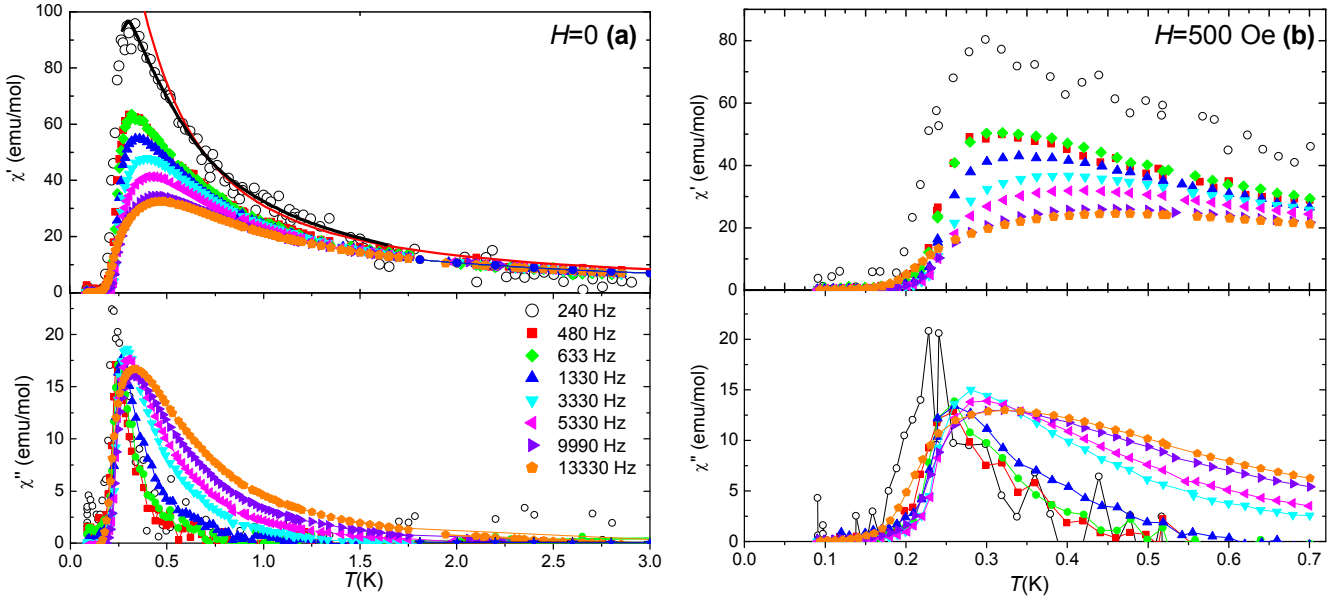

Fig. 7. Real and imaginary components of the susceptibility measured at low temperatures in a dilution refrigerator at $H_{ac}=4$ Oe and different frequencies f: (a) At $H=0$. The low frequency $\chi''(T)$ curve between 0.6 K<T<3K has been fitted using, i) Red thin line: the Ising $S^*=1/2$ ABC model, with $J'/k_B=J''/k_B=+0.55$ K; ii) Black thick line: Navarro's model for an Ising chain of $S^*=1/2$ spins, Eq. [13], with intrachain $J'/k_B=+0.528(1)$ K and interchain coupling $J'''/k_B=-0.021(2)$ K; (b) Data at dc field $H=500$ Oe.

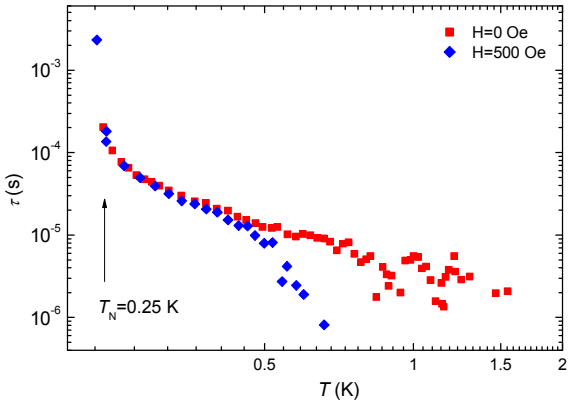

Fig. 8. Low temperature relaxation time, τ, as determined from χ'(T) and χ''(T) at H=0 and H=500 Oe.

coupling constants. A nice fit of the experimental data is achieved (Fig. 7a), with the predicted peak χ'_{max}=96.8 emu/mol (at T_N=0.29 K) very close to the experimental values, with the coupling constants $J'/k_B \equiv J''/k_B$=+0.528(1) K and J'''/k_B= -0.021(1) K. These values are in agreement with those obtained in the magnetic heat capacity analysis.

The $\chi'(T)$ and $\chi''(T)$ curves measured between 85 mK <T<3.0 K in a dilution refrigerator exhibit slow relaxation (Fig. 7a). In the range 0.6<T<3.0 K, the relaxation rate was estimated as $\tau(T)= \chi''/(\chi'-\chi_s)\omega$, using data measured at the frequency f=1.3 kHz fulfilling the condition $\omega\tau \approx 0.1 << 1$ ($\omega = 2\pi f$), and the adiabatic limit of the susceptibility, χ_s. As can be observed in Fig. 8, τ is very fast ($\tau_T \approx 10^{-5}$ s), and practically temperature-independent, indicating that spin reversal probably occurs through quantum tunneling (QT), at least, down to 0.6 K.

In the present Dy compound, according to the *ab initio* calculations, the anisotropy barrier to rotation has been found to be of Δ/k_B=73.4 K. Since Dy(III) ground state is a Kramers doublet, quantum tunneling through the degenerate states is only possible thanks to the dipole-dipole and exchange interactions, and non-local symmetry, which introduce a perturbation in the Hamiltonian that allows the mixing of the two states. We denominate this effect by the generic term of dipolar bias, at this stage. At very low temperature, but above T_N, i.e. in the paramagnetic region, the relaxation process may be pure quantum tunneling (QT) process, through the ground state, not assisted by phonons [33]. The probability of this process depends on the distribution of dipolar energy bias, $P(\xi_{dip})$. Dipolar fields split the ground state doublet by the amount $\Delta E = (\Delta_T^2 + \xi^2)^{1/2}$, where $\Delta_T = g^*_{xy}\mu_B H_{dip,xy}$ is the quantum tunnel splitting, $\xi = g^*_z \mu_B H_{dip,z}$ is the dipolar bias and g^*_z and g^*_{xy} are the longitudinal and perpendicular g^* tensor components. At zero field, only the small fraction of clusters fulfilling the condition $\Delta_T \geq \xi_{dip}$ can reverse its magnetic moment at any given time, then the tunneling time τ_T depends on the distribution of dipolar (or exchange) energy bias $P(\xi_{dip})$ and on the quantum tunnel splitting Δ_T [34]:

$$\tau_T \approx \frac{\hbar}{\Delta_T^2 P(\xi_{dip})} . \qquad [13]$$

At H=0, the energy bias distribution may be approximated to a Gaussian $P(\xi_{dip}=0) = 1/\sqrt{2\pi}\sigma_{\xi dip}$, where the width $\sigma_{\xi dip}$ can be estimated from the condition $\sigma_{\xi dip} \approx k_B T_N$ =0.25 K. The width of the bias field is estimated to be $\sigma_{dip,z} = \sigma_{\xi,dip} / g^*_z \mu_B \approx 200(20)$ Oe. (Although it could be larger than 200 Oe because of the intrachain mean field increasing as the short range order sets on in the neighborhood of T_N). By substitution in Eq. [13] one obtains the value $\Delta_T / k_B \approx 7x10^{-4} K$. These can be compared to the values $\sigma_{dip,z} = 500$ Oe and $\Delta_T / k_B \approx 2x10^{-4} K$ found in $\{Dy(\alpha-fur)_3\}_n$ complex, where Dy has a similar environment [5].

It should be remarked that the imaginary susceptibility at f=240 Hz and zero field, $\chi''(T)$ shows a peak at T_N. Since the system is nearly in thermal equilibrium at this frequency, this feature implies that upon magnetic ordering magnetic domains with non-zero magnetization are created, giving rise to energy absorption when excited with the ac field. Since the long-range magnetic ordering is fundamentally antiferromagnetic, the domains may originate from several sources; the spins at the antiferromagnetic domain walls [35], the domain motions within the ferromagnetic chains [14], or a non-compensated weak ferromagnetic component [36, 37, 38]. As frequency increases, the spin system is no longer in isothermal equilibrium conditions and the peak becomes a maximum that shifts towards higher temperatures as frequency increases. This is indicative of a slowing down in the dominant relaxation rate τ_T^{-1}.

This is confirmed by the temperature dependence of the spin-lattice relaxation time, τ, as determined from the susceptibility data measured at fixed f=1.3 kHz, that is shown in Fig. 8. As temperature approaches T_N, τ rapidly increases, thus showing a rapid slowing down of the QT dynamics in the vicinity of the magnetic phase transition. This effect can be classified as a *critical slowing down* in terms of magnetic phase transition theory [39, 6], though in this case the thermal fluctuations have quantum tunneling as origin. The reason for this effect is the narrowing of the distribution $P(\xi_{dip})$ and its maximum shift from ξ_{dip}=0 to $\xi_{dip} \approx k_B T_N$, generating a net bias field; i.e. at a local spin scale it implies the appearance of an internal field that tends to detune the ground state spin levels that gave rise to the QT process. As a consequence the relaxation time slows down. Such a critical slowing down has been observed earlier near the long range magnetic ordering temperature in crystals of ErW_{10} [33].

Field-dependence. Fig. 7(b) shows χ', $\chi''(T)$ dynamic measurements performed in the low temperature range (85 mK<T<3.0 K) under a constant field H=500 Oe. The antiferromagnetic long-range order takes place at T_N=0.23 K. Thus, essentially, the same behavior as that observed for H=0 is found, though slightly shifted to lower temperature. We note that at this field no metamagnetic transition to a ferromagnetic phase takes place. To explain this feature, we have to consider that the sample is a randomly oriented powder and only a small fraction of the spins undergo the metamagnetic transition, thus the transited ferromagnetic to antiferromagnetic volume ratio in the sample is small, and the antiferromagnetic behavior dominates. Besides, effective field acting on the Dy is the internal field, which is smaller than the applied because of the demagnetizing factor [40]. Both effects cooperate in avoiding the observation of the transited fraction of the sample. Thus, it is concluded that this field does not modify fundamentally the processes active at these low temperatures.

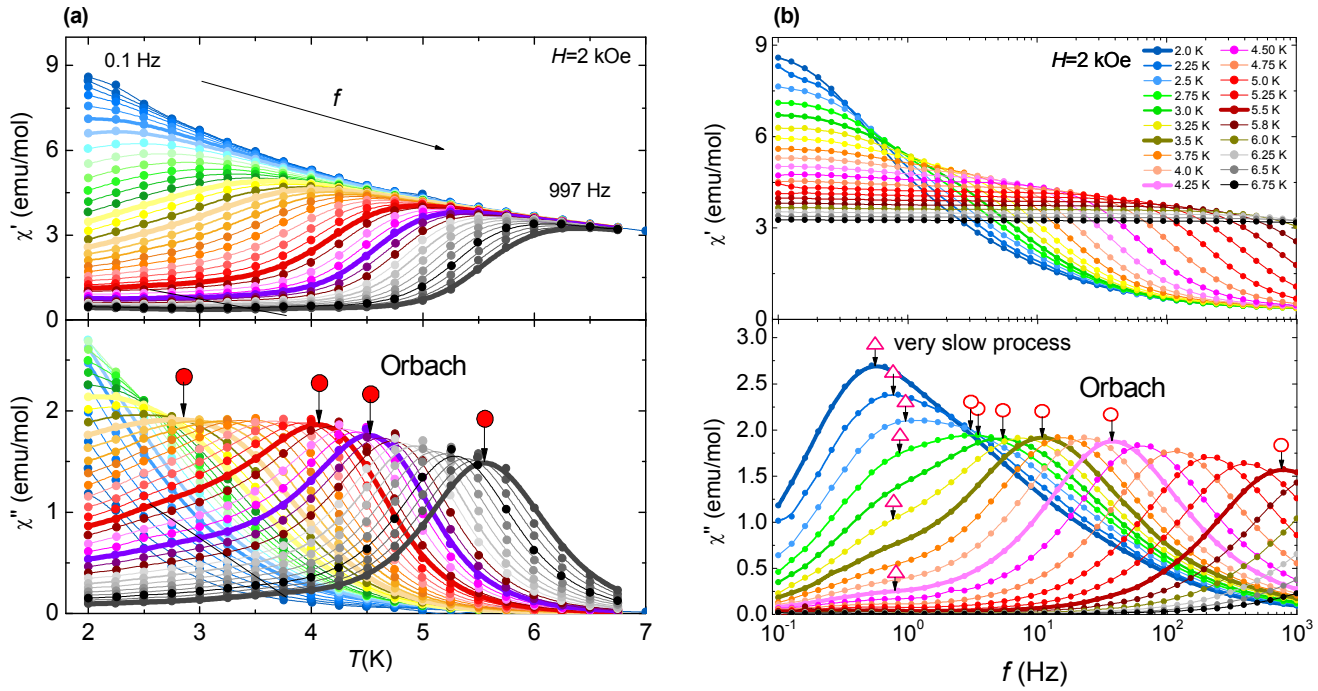

Fig. 9. (a) χ', χ''(T) at different frequencies at applied field H=2 kOe; (b) same data represented as χ', χ''(f) at different temperatures.

B. Temperature range 3 K<T<8 K

Zero-field. The susceptibility curves measured by SQUID magnetometry in this range did not show any frequency dependence (Fig. S3a).

Field dependence. χ'(T) and χ''(T) measurements were performed at a constant applied field H=2 kOe, at different frequencies between 0.1-997 Hz (Fig. 9a). The same data was represented as χ'(f) and χ''(f), at different fixed temperatures, to help discerning all possible relaxation processes in the system (Fig. 9b). Figure 10b summarizes the relaxation time as a function of 1/T and intensity of all the χ'' peaks observed.

The χ''(T) plot (Fig. 9a) evidences the existence of a relaxation process (bold circles), which follows a linear $\ln\tau(1/T)$ dependence for temperatures T<4.6 K, and may be assigned to the spin reversal of each of the individual Dy's by an Orbach process, with an activation energy U/k_B=68(3) K and characteristic time τ_0=1.0(1)x10^{-9}s. This activation energy value is very close to the zero-field splitting energy Δ/k_B=73.4 K, calculated in Section IV.

On the other hand, the χ''(f) representation shown in Fig. 9b presents a χ'' peak shifting to lower frequencies for decreasing temperatures (red open circles), and a practically T-independent peak at very low frequency, with intensity rapidly growing with decreasing T (red open triangles). The first relaxation process corresponds to the Orbach process already identified in the χ''(T) plot. At temperatures T<4.6 K, $\ln\tau$ *vs.* 1/T deviates from linearity, and simultaneously, a very slow process, with a close to constant relaxation rate τ_s≈0.2 s, gains intensity.

In order to further investigate the evolution with the field of the two identified relaxation processes, χ', χ''(f) measurements as a function of the field between 0-40 kOe were performed at constant temperatures, T=4.0 K and T=2.5 K. (Fig. S4). Figure 10 (a and c) shows the field dependence of the two different relaxation processes at these two temperatures. At both temperatures, no relaxation is observed at H=0. For H≠0 and

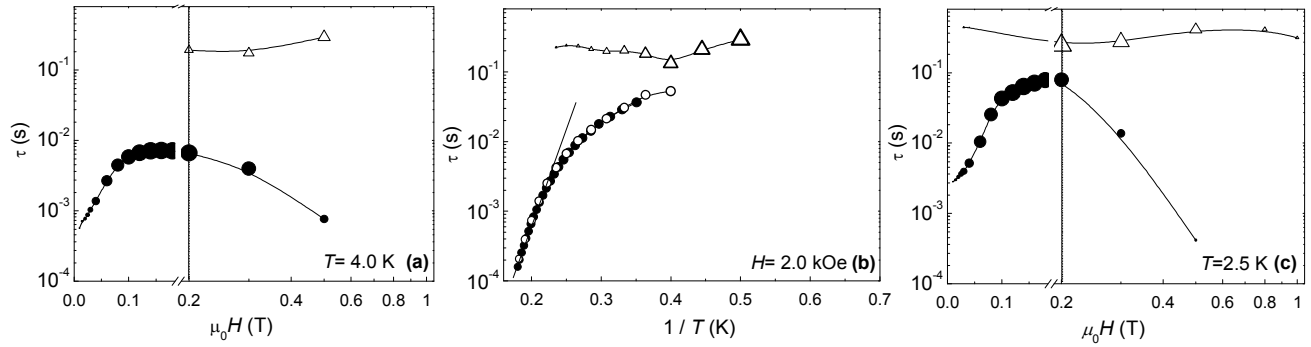

Fig. 10. Central panel: Relaxation time as a function of the inverse temperature, $\tau(1/T)$, obtained at H=2 kOe (b). Lateral panels: Relaxation time as a function of the applied field, $\tau(H)$, at T=4 K (a) and T=2.5 K (c).

increasing field the relaxation peak ascribed to the Orbach process grows and the relaxation time increases till reaching a maximum; at higher fields the Orbach peak looses intensity and the relaxation time decays, while a second, very slow process appears with increasing intensity as temperature decreases.

In other Dy SIM compounds, [Dy(COT'')2Li(THF)-(DME)] [41] and Dy(III)-DOTA [42], it has been reported that an applied field opens multiple relaxation channels. Moreover, very slow magnetic relaxation has been reported earlier in SIMs, and is ascribed to direct phonon-induced process [5], Orbach processes involving excited Kramers doublets [43], Resonant Phonon Trapping (RPT) or phonon bottleneck effects [44]. Although our system fulfills the conditions under which RPT may occur [45], the phenomenology observed in our complex does not match with that reported for other SIMs with RPT-slow relaxation. First, in our complex τ_s is nearly independent of T, while RPT mechanism leads instead to $\tau_{RPT} \alpha T^{-2}$. Second, the observed slow process emerges as the QT process fades out with increasing field, whereas the RPT mechanism is expected to occur already at zero-field and show a τ_{RPT} versus field dependence [44] different from that observed in our experiments.

Hence, the very slow relaxation process in our complex is of spin-phonon, rather than spin-spin, type, and its contribution to the overall magnetic relaxation is enhanced with decreasing temperature as the population of the lowest energy phonon modes increases.

The magnetic relaxation of our complex is similar to that earlier reported for another α-fur based complex, $\{Dy(\alpha\text{–}fur_3)\}_n$ [5], where the very slow process was ascribed to spin reversal through a direct process, presenting a characteristic $\tau_D(H) \alpha H^{-4}$ dependence at high fields. Unfortunately, in the present compound, this field dependence could not be observed within the measurement window, so the origin of the slow relaxation processes cannot be completely ascertained.

VIII. Molecular field-biased double switch

In the previous section it was shown that the application of a H=2 kOe field quenches the fast QT process, and forces the system to relax via alternative processes which can be up to 5 orders of magnitude slower, depending on the temperature of work. We propose that this effect may be profited to design a molecular on/off field-biased switch, as demonstrated here.

In the experiment shown in Fig. 11a, the susceptibility was recorded at T=4 K as a function of the frequency, while the field was reversibly switched between 0 and 2 kOe at intervals of about half a decade. At this temperature, magnetic relaxation processes under the application of a 2 kOe take place via two available pathways: a very slow process, with a relaxation time of τ_s=0.2 s, and an Orbach process, with τ_{or}=6x10^{-3} s (at T=4 K), (Fig. 11b). When the field is removed the relaxation time falls abruptly to $\tau_{QT} \approx 10^{-5}$ s and the χ'' signal becomes negligible. Thus, two different switches are available at once, which can be selected by tuning the frequency bias. The "slow process-QT" switch has a large τ gap (5 orders of magnitude) and small signal difference (~0.4 emu/mol) between the on/off states, whereas the "Orbach-QT" switch has a smaller τ gap (about 3.5 orders of magnitude) but larger amplitude difference (~2 emu/mol).

In a previous work, Han *et al.* [11h] reported a family of Dy_2-complexes where slow relaxation was switched on/off by modulating the packing mode and ligand field. In the device we propose now, the switch can be externally triggered by an applied field.

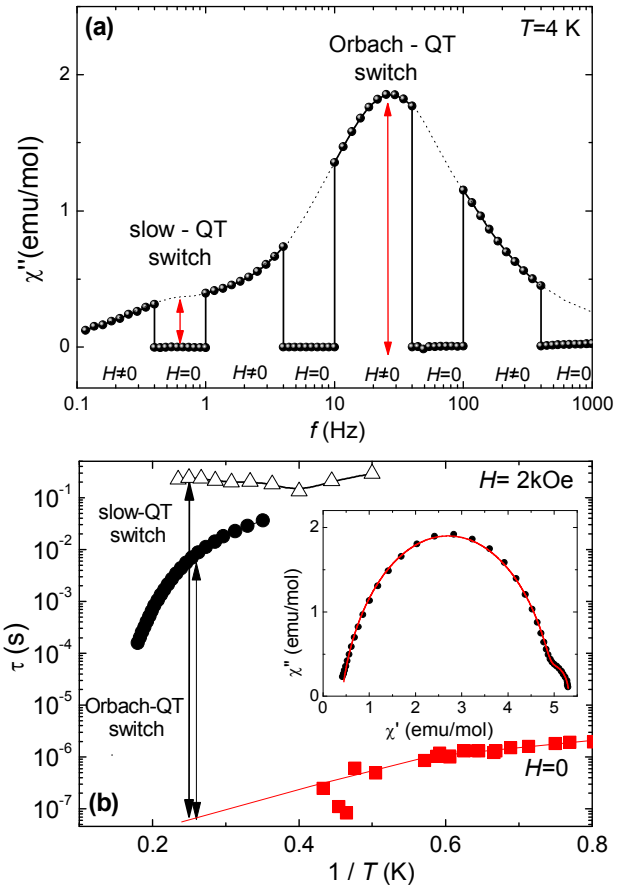

Fig. 11 . On-off switching of the slow relaxation by H biasing: (a) Imaginary susceptibility as a function of the frequency at T= 4 K, as the field H is alternatively switched on (H=2 kOe) and off (H=0); (b) Relaxation time τ as a function of 1/T: the arrows signal the $\Delta\tau$ between the ultrafast τ_{QT} process and each one of the available slow relaxation paths, with τ_{or}, τ_s, at 4 K, achieved by switching the field on. Inset: Cole-cole plot of susceptibility data at 4 K, 2 kOe and fit to a double-Debye function.

The proposed molecular device may work in different modes: (i) to switch the signal between two different states (χ''=0, χ''≠0), in the philosophy of magnetic switching of multiferroic materials [46a] or resistive memories [46b]; or perhaps more interestingly, (ii) to switch the response between a fast and a slow mode, as if it were a molecular "gearshift", with application e.g. in digital frequency modulated signal transmission.

IX. Discussion and Conclusions

The main objective of this work is to study the competing effects of (i) SIM local fluctuations which promote to paramagnetic behavior, and (ii) Dy-Dy interactions which tend to provoke long range-order. For this purpose, the dynamic results on $\{Dy_2Ba(\alpha\text{-}fur)_8.2H_2O\}_n$ (**1**) are extensively described, and compared to those of the related furoate $\{Dy(\alpha\text{-}fur)_3\}_n$ **(2).**

The polymeric compound (**1**) has been synthesized and structurally characterized. X-ray diffraction shows that the complex is formed by the assembly of 1D zig-zag chains of Dy_2 dimers separated by Ba ions, running along the *c*-axis. *Ab initio* calculations have been performed to determine the axes of the

gyromagnetic tensor. A large magnetic anisotropy of the ground state has been found (g_z*=18.7 >>g_x*=0.1, g_y*=0.3).

From the fit to heat capacity and susceptibility data we have found that the magnetic behavior corresponds to that of an Ising, S*=1/2, alternating bond chain model system, where the intradimer and interdimer interactions are both ferromagnetic, and of the same order, $J'/k_B = J''/k_B$=+0.528 K. At T_N=0.25 K the compound undergoes an antiferromagnetic long-range ordering. The interchain interaction has been estimated as J'''/k_B=-0.021(2).

Combining all the information, structural, magnetic and computational, obtained in this work we may propose that the low temperature, ordered magnetic structure consists of ferromagnetically coupled zig-zag chains, constituted by dimeric sections. The Dy(III) moments in a chain are parallel and contained in the *bc*-plane. In addition, due to the crystal symmetry, the easy magnetic axes for Dy(III) ions on alternate planes along the *b*-axis are canted 68º between them, being the *c*-axis almost the bisector line of such angle, as shown in Fig. 3b, The adjacent chains in the *ac*-plane are antiferromagnetically oriented.

Assuming that below T_N the ordered magnetic structure is the one conjectured above, the dipolar interactions (through space) of one Dy with its first neighbors have been calculated, expressed in terms of the S*=1/2 model, with the expression:

$$U_{dip,i} = -2J_{dip}\vec{S}^{*}.\vec{S}_i^{*} = -\frac{\mu_0}{4\pi}\frac{3(\vec{m}.\vec{r}_i)(\vec{m}_i.\vec{r}_i) - r_i^2(\vec{m}.\vec{m}_i)}{r_i^5} \quad [14]$$

where $\vec{m} = \hat{g}^{*}\vec{S}^{*}$, and $\hat{g}^{*}$ is the gyromagnetic tensor [47].

In Table 3 the dipolar interaction constant J_{dip} to the next neighbor Dy moments is shown, in comparison with the values derived from the fit to the model described in Section V.

The strength of the intradimer interaction is very close to the predicted sign and value for only dipolar interaction (J'_{dip}=+0.623 K) (see Table 3). The predicted value for J''_{dip} and J'''_{dip} are too low and too high, respectively, though of the correct sign and order of magnitude. In the first case, J'', the difference should be due to the contribution of the superexchange magnetic interaction. As for the interchain interaction, J''', the value for the fit has been obtained considering 4 neighbours whereas the dipolar contribution has been calculated for only the closest pair of Dy-Dy on different chains. Although we expect J''' being purely of dipolar nature, dipolar interactions are actually long range. There are positive and negative compensating contributions for Dy atoms laying at further distances, that would reduce the total dipolar interaction, thus explaining the difference in J'''.

The intradimer coupling constant in this complex is relatively small, compared to other dinuclear Dy complexes. In Table S1 we present a summary of reported ferro- and AF Dy_2-complexes,

	d(Å)	J_{dip}(K)	J(K)
Intradimer J'/k_B	4.471	0.623	0.528(1)
Interdimer J''/k_B	8.176	0.117	0.528(1)
Interchain J'''/k_B	7.977	-0.051	-0.021(2)

Table 3. Summary of intradimer, interdimer and interchain interactions of dipolar type, calculated by considering the magnetic moments as Ising spins oriented along the directions of the easy magnetic axes, obtained from the *ab initio* calculations, The fit parameters obtained from the fit to the ABC model proposed in Section V are also shown for comparison.

where the type of Dy-Dy bridge, the intradimer Dy distance and angle, together with the intradimer coupling constants have been collected from the literature. For $\{Dy_2Ba(\alpha\text{-fur})_8\}_n$ the intradimer distance is the largest among all the complexes. The ferromagnetic exchange is mediated by two Dy-O-C-O-Dy bridges provided by the α-fur ligands, and this indirect path via carbon atoms leads to a much weaker ferromagnetic coupling than the Dy-O-Dy paths existing in other complexes.

The magnetic dynamics of this compound change as the temperature is decreased and the thermally activated processes are progressively quenched. The slowing down of the relaxation processes induced by the internal and the applied fields has the effect of rounding the maxima of the $\chi'(T)$ and $\chi''(T)$ curves near T_N. However, the phase transition to the AF ordered state is not quenched and manifests itself in a very abrupt decrease of the ac susceptibility below T_N=0.25 K. Therefore, the Dy-Dy interactions, though weak, dominate at low enough temperature over any remaining fluctuation, of thermal or quantum origin, and establish long-range magnetic ordering at T_N.

We compare now the similitudes and differences between the magnetic static and dynamic properties of $\{Dy_2Ba(\alpha\text{-fur})_8.2H_2O\}_n$ **(1)** and the previously studied $\{Dy(\alpha\text{-fur})_3\}_n$ **(2)** [5] (see Fig. 12 and Table S3). At H=0 their electronic level scheme consists of Kramers doublets. In both compounds the coordination number of oxygen atoms is eight, although the coordination polyhedra are different: a distorted square antiprism in **(1)** and a distorted bicapped trigonal prism in **(2)**. Moreover, in **(2)** two different sites for Dy exist.

This gives rise to different zero-field splitting energies, Δ/k_B=68 K in **(1)**, and 38 K (site DyA), 79 K (site DyB) in **(2)**. In both compounds the gyromagnetic tensor components indicate strong uniaxial anisotropy, with small, but non-negligible transverse components: g_y*=0.3 and 0.1 for **(1)** and **(2)** DyB. Both compounds have static ferromagnetic chain behavior undergoing antiferromagnetic ordering at T_N=0.25 K and 0.668 K, for compounds **(1)** and **(2)**, respectively.

However, the dynamical properties are quite different. At H=0, within the frequency windows used in these works (SQUID: $0.1<f<10^3$ Hz, PPMS and home-built very low temperature susceptometer; $10<f<10^5$ Hz) just a very fast relaxation due to QT is detected in **(1)**, with a critical slowing down of QT when T approaches T_N. In contrast, above 4 K, in **(2)** for both sites, DyA and DyB, thermal activated quantum tunneling (TAQT), with an activation energy, Δ/k_B, that corresponds to the energy difference between the ground state and the first excited level is observed. Since Δ/k_B is very similar in complexes **(1)** and **(2)** for site DyB, the 30-fold shorter QT relaxation time of complex **(1)** cannot be attributed to a very different anisotropy hindering barrier. Instead, the difference can be explained by the difference in bias field $\sigma_{dip,z}$ and transverse component of the $\hat{g}^{*}$ tensor (g_y*), that leads to a different Δ_T. Indeed, from Eq. 13 one derives: $\tau_T \propto \sigma_{dip,z} / \Delta_T^2$. Then, substituting the parameters for the two compounds (see Table S3) one obtains a relaxation τ_T shorter by a factor 30 in **(1)** with respect to that of site DyB in **(2)**, which agrees nicely with the experiment (see Table S3).

Both compounds (**1**) and (**2**) show slowing down of τ_T when approaching T_N, however, it is in (**1**) where this effect is more clearly resolved (see Fig. 12). At H=0 there is a competition between: (i) spin reversal fluctuations caused by tunneling processes within the ground doublet [48], that provide a mechanism allowing the system to reach equilibrium, and (ii) the short-range correlations caused by exchange or dipolar interactions, that polarize progressively the spins in the system as

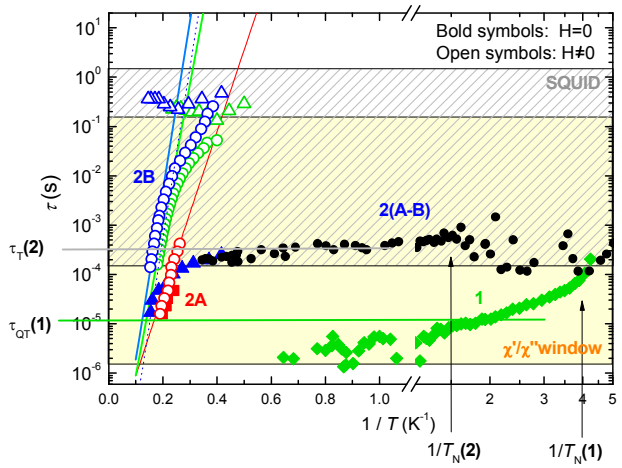

Fig. 12. Comparison between the relaxation data, $\tau(1/T)$, determined for $\{Dy_2Ba(\alpha\text{-fur})_8.2H_2O\}_n$ complex **(1)** (green) and the previously studied complex $\{Dy(\alpha\text{-fur})_3\}_n$ **(2)** [5], containing two different Dy sites (A: red) and (B: blue). Black symbols correspond to an average relaxation time for sites A and B. Data were collected at H=0 (bold symbols) and $H\neq0$ (2-4 kOe) (open symbols). The grated yellow and plain yellow areas correspond to the frequency windows for SQUID, PPMS and very low temperature ac susceptometers, respectively.

the correlation length tends to infinity at T_N [6]. The slowing down of τ_T in both complexes is caused by mechanism (ii), and since the interaction J''' is smaller in **(1)**, it extends down to lower temperature (see Fig. 12).

Because of the extended temperature region and the much lower τ_T of **(1)** with respect to **(2)** above T_N, the critical slowing down of τ_T as T approaches T_N is clearly discernible in **(1)**. The increasing local internal field, of dipolar and exchange origin, tends to quench the tunneling process as the short range correlation length tends to infinity at T_N. Thus we have proved that different dynamics are caused by the different relative strengths of the two competing effects in Dy(III) SIMs that are otherwise nearly identical at the atomic level.

For $H\neq0$, in both **(1)** and **(2)** (DyA and B sites), an Orbach process; i.e. a relaxation time τ_{or} that follows an Arrhenius law temperature dependence with activation energies very close to the gap energy Δ/k_B, are observed. Moreover, in **(1)** and **(2)** a very slow relaxation process appears, at the expense the other slow process, with a nearly temperature independent characteristic relaxation time $\tau_s\approx2\text{-}4x10^{-1}$ s. This latter process is assigned to the direct relaxation mechanism due to the lifting of the Kramers degeneracy on the ground state. So, the external field has the effect of quenching the QT and TAQT processes by detuning the levels through which tunnelling takes place.

In summary, it is concluded that both compounds have SIM behavior, although in **(1)** slow relaxation needs to be induced by an applied field, while in **(2)** it appears already at H=0. The measurements of SIMs at temperatures below 1 K, have allowed us to observe the critical slowing down in the quantum tunneling fluctuations caused by magnetic correlations towards 3D ordering near T_N.

.

Acknowledgements

This work has been financed by MECOM Projects MAT11/23791 and MAT11/27233-C02-02, MAT2012-38318-C03, DGA IMANA Project E34, MOLCHIP Project E98Consolider Nanoselect (CSD2007-00041) and by a grant of the Ministry of National Education, CNCS – UEFISCDI, project number PN-II-ID-PCE-2012-4-0261. The authors thankfully acknowledge the resources from the supercomputer "Caesaraugusta" (node of the Spanish Supercomputer Network), technical expertise and assistance provided by BIFI - Universidad de Zaragoza.

References

1 N. Ishikawa, M. Sugita, T. Ishikawa, S. Koshihara, and Y. Kaizu, *J. Am. Chem. Soc*., 2003, **125**, 8694.

2 M. Ganzhorn and W. Wernsdorfer, , in *Molecular magnets, Physics and Applications*, NanoScience and Nanotechnology, 2013 Springer V. Series on Heidelberg New-York Dordrecht London (DOI 1007/978-3-642-40609-6), Ch. 13.

3 (a) L. Sorace, C. Benelli and D. Gatteschi, *Chem. Soc. Rev*., 2011, **40**, 3092; (b) R. J. Blagg, F. Tuna, E. J. L. McInnes and R. E. P. Winpenny, *Chem. Commun*., 2011, **47**, 10587.

4 (a) D. Gatteschi, *Nat. Chem*., 2011, **3**, 830; (b) Y. N. Guo, G. F. Xu, Y. Guo and J. Tang, *Dalton Trans.*, 2011, **40**, 9953; (c) Y.-Z. Zheng, Y. Lan, W. Wernsdorfer, C. E. Anson and A. K. Powell, *Chem.-Eur. J.,* 2009, **15**, 12566; (d) D. Aguila, L. A. Barrios, F. Luis, A. Repolles, O. Roubeau, S. J. Teat and G. Aromí, *Inorg. Chem*., 2010, **49**, 6784; (e) S. A. Sulway, R. A. Layfield, F. Tuna, W. Wernsdorfer and R. E. Winpenny, *Chem. Commun*., 2012, **48**, 1508; (f) J. Tang, I. Hewitt, N. T. Madhu, G. Chastanet, W. Wernsdorfer, C. E. Anson, C. Benelli, R. Sessoli and A. K. Powell, *Angew. Chem., Int. Ed.,* 2006, **45**, 1729; (g) H. Ke, P. Gamez, L. Zhao, G.-F. Xu, S. Xue and J. Tang, *Inorg. Chem.,* 2010, **49**, 7549; (h) M. T. Gamer, Y. Lan, P. W. Roesky, A. K. Powell and R. Clérac, *Inorg. Chem*., 2008, **47**, 6581; (i) P. Zhang, Y.-N. Guo and J. Tang, *Coord. Chem. Rev*., 2013, **257**, 1728.

5 E. Bartolomé, J. Bartolomé, S. Melnic, D. Prodius, S. Shova, A. Arauzo, J. Luzón, F. Luis and C. Turta, *Dalton Trans*., 2013, **42**, 10153.

6 F. Luis, in *Molecular magnets, Physics and Applications*, NanoScience and Nanotechnology, 2013 Springer V. Series on Heidelberg New-York Dordrecht London (DOI 1007/978-3-642-40609-6), Ch. 7, 161.

7 (a) C. Turta, S. Melnic, M. Bettinelli, S. Shova, C. Benelli, A. Speghini, A. Caneschi, M. Gdaniec, Yu. Simonov, D. Prodius and V. Mereacre, *Inorg. Chim. Acta*, 2007, **360**, 3047; (b) S. Melnic, D. Prodius, S. Shova, H. Stoeckli-Evans, Yu. Simonov, A. Feher, M. Gdaniec and C. Turta, *Chem. J. Moldova*, 2009, **4**, 60; (c) L. V. Mingalieva, V. K. Voronkova, R. T. Galeev, A. A. Sukhanov, S. Melnik, D. Prodius and K. I. Turta, *Appl. Magn. Reson*., 2010, **37**, 737; (d) S. Melnic, D. Prodius, H. Stoeckli-Evans, S. Shova and C. Turta, *Eur. J. Med. Chem*., 2010, **45**, 1465; (e) S. Melnic, D. Prodius, Ch. Simmons, L. Zosim, T. Chiriac, V. Bulimaga, V. Rudic and C. Turta, *Inorg. Chim. Acta*, 2011, **373**, 167.

8 D. Aguilà, L. A. Barrios, V. Velasco, L. Arnedo, N. Aliaga-Alcalde, M. Menelaou, S. J. Teat, O. Roubeau, F. Luis and G. Aromí, *Chem. -Eur. J*., 2013, **19**, 5881.

9 F. Habib and M. Murugesu, *Chem. Soc. Rev*, 2013, **42**, 3278.

10 (a) Y. N. Guo, G. F. Xu, W. Wernsdorfer, L. Ungur, Y. Guo, J. Tang, H. Zhang, L. F. Chibotaru and A. K. Powell, *J. Am. Chem. Soc.*, 2011, **133**, 11948; (b) X. Yi, K. Bernot, O.

Cador, J. Luzón, G. Calvez, C. Daiguebonne and O. Guillou, *Dalton Trans.*, 2013, **42**, 6728; (c) M. Ren, S. S. Bao, N. Hoshino, T. Akutagawa, B. Wang, Y. C. Ding, S. Wei and L. M. Zheng, *Chem.-Eur. J.*, 2013, **19**, 9619; (d) P.-H. Lin, W.-B. Sun, M. –F. Yu, G. –M. Li, P. –F. Yan and M. Murugesu, *Chem. Commun*., 2011, **47**, 10993; (e) P. –H. Lin, T. J. Burchell, R. Clérac and M. Murugesu, *Angew. Chem., Int. Ed*., 2008, **47**, 8848; (f) Y. -N. Guo, X. -H. Chen, S. Xue and J. Tang, *Inorg. Chem*., 2011, **50**, 9705; (g) G. –F. Xu, Q. –L. Wang, P. Gamez, Y. Ma, R. Clérac, J. Tang, S. –P. Yan, P. Cheng and D. –Z. Liao, *Chem. Commun*., 2010, **46**, 1506; (h) S. J. Liu, J. P. Zhao, W.C. Song, S.D. Han, Z.Y. Liu and X. H. Bu, *Inorg. Chem.*, 2013, **52**, 2103; (i) K. Bernot, F. Pointillart, P. Rosa, M. Etienne, R. Sessoli and D. Gatteschi, *Chem. Commun*., 2010, **46**, 6458.

11 (a) F. Tuna, C. A. Smith, M. Bodensteiner, L. Ungur, L. F. Chibotaru, E. J. L. McInnes, R. E. P. Winpenny, D. Collison and R. A. Layfield, *Angew. Chem.,* 2012, **124**, 7082; (b) J. D. Rinehart, M. Fang, W. J. Evans and J. R. Long, *Nat. Chem.,* 2011, **3**, 538; (c) X. Yi, K. Bernot, F. Pointillart, G. Poneti, G. Calvez, C. Daiguebonne, O. Guillou, R. Sessoli, *Chem.-Eur. J.*, 2012, **18**, 11379; (d) S. Demir, J. M. Zadrozny, M. Nippe and J. R. Long, *J. Am. Chem. Soc.*, 2012, **134**, 18546; (e) J. Long, F. Habib, P. –H. Lin, I. Korobkov, G. Enright, L. Ungur, W. Wernsdorfer, L. F. Chibotaru and M. Muguresu, *J. Am. Chem. Soc*., 2011, **133**, 5319; (f) Y. Ma, G. F. Xu, X. Y, L. C. Li, J. Tang, S.P. Yan, P. Cheng and D. Z. Liao, *Chem. Commun.* 2010, **46**, 8264; (g) F. Pointillart, Y. L. Gal, S. Golhen, O. Cador and L. Ouahab, *Chem.-Eur. J*., 2011, **17**, 10397; (h) T. Han, W. Shi, X. Zhang, L. Li and P. Cheng, *Inorg. Chem*., 2012, **51**, 13009; (i) F. Habib, P. –H. Lin, J. Long, I. Korobkov, W. Wernsdorfer and M. Murugesu, *J. Am. Chem. Soc*., 2011, **133**, 8830; (j) Y. –N. Guo, G. –F. Xu, Y. Guo *et al*., *Dalton Trans.*, 2011, **40**, 9953; (k) V. Patroniak, P. N. W. Baxter, J. -M. Lehn, Z. Hnatejko and M. Kubicki, *Eur. J. Inorg. Chem.*, 2004, **11**, 2379.

12 (a) L. Bogani, C. Sangregorio, R. Sessoli and D. Gatteschi, *Angew. Chem., Int. Ed.,* 2005, **44**, 5817; (b) H. Miyasaka, T. Nezu, K. Sugimoto, K. Sigiura, M. Yamashita and R. Clérac, *Chem.-Eur. J*., 2005, **11**, 1592; (c) L. Lecren, W. Wernsdorfer, Y. G. Li, A. Vindigni, H. Miyasaka and R. Clérac, *J. Am. Chem. Soc*., 2007, **129**, 5045; (d) H. Miyasaka, A. Saitoh, M. Yamashita and R. Clérac, *Dalton Trans.,* 2008, **18**, 2422; (e) M. Ferbinteanu, H. Miyasaka, W. Wernsdorfer, K. Nakata, K. Sugiura, M. Yamashita, C. Coulon and R. Clérac, *J. Am. Chem. Soc*., 2005, **127**, 3090.

13 T. Han, W. Shi, Z. Niu, B. Na and P. Cheng, *Chem.-Eur. J*., 2012, **19**, 994.

14 R. J. Glauber, *J. Math. Phys*., 1963, **4**, 294.

15 D. Visinescu, A. M. Madalan, M. Andruh, C. Duhayon, J. –P. Sutter, L. Ungur, W. van den Heuvel and L. F. Chibotaru, *Chem. –Eur. J.*, 2009, **15**, 11808.

16 L. Bogani, A. Vindigni, R. Sessoli, and D. Gatteschi, *J. Mater. Chem.*, 2008, **18**, 4750.

17 R. Inglis, L. F. Jones, K. Mason, A. Collins, S. A. Moggach, S. Parson, S. P. Perlepes, W. Wernsdorfer, and E. K. Brechin, *Chem. –Eur. J*., 2008, **14**, 9117.

18 (a) D. -L. Long, A. J. Blake, N. R. Champness, C. Wilson, and M. Schröder, *Chem. -Eur. J.*, 2002, **8**, 2026; (b) F. –S. Guo, J. –D. Leng, J. –L. Liu, Z. –S. Meng, and M. –L. Tong, *Inorg. Chem.*, 2012, **51**, 405.

19 D. Visinescu, I. –R. Jeon, A. M. Madalan, M. –G. Alexandru, B. Jurca, C. Mathonière, R. Clérac, and M. Andruh, *Dalton Trans*., 2012, **41**, 13578.

20 T. Han, W. Shi, Z. Niu, B. Na, and P. Cheng, *Chem. Eur. J*., 2013, **19**, 994.

21 (a) M. L. Kahn, P. Lecante, M. Verelst, C. Mathonière and O. Kahn, *Chem. Mater*., 2000, **12**, 3073; (b) M. Evangelisti, M. L. Kahn, J. Bartolomé, L. J. de Jongh, C. Meyers, J. Leandri, Y. Leroyer and C. Mathonière, *Phys. Rev. B*, 2003, **68**, 184405; (c) X. Li, X. –S. Wu, H. –L. Sun, L. –J. Xu and G. –F. Zi, *Inorg. Chim. Acta*, 2009, **362**, 2837.

22 S. Zhang, Y. Wang, J. Zhao, P. Ma, J. Wang and J. Niu, *Dalton Trans.*, 2012, **41**, 3764.

23 L. Sun, G. -Z. Li, M. –H. Xu, X. –J. Li, J. –R. Li and H. Deng, *Eur. J. Inorg. Chem.*, 2012, 1764.

24 H. Miyasaka and M. Yamashita*, Dalton Trans.*, 2007, **4**, 399.

25 CrysAlis RED, Oxford Diffraction Ltd., Version 1.171.34.76, 2003.

26 (a) F. L. Mettes, PhD Thesis, Leiden, 2001; (b) Y. E. Volokitin, PhD Thesis, Leiden, 1997.

27 B. O. Roos and P. A. Malmqvist, *Phys. Chem. Chem. Phys.,* 2004, **6**, 2919.

28 F. Aquilante, L. De Vico, N. Ferre, G. Ghico, P. A. Malmqvist, P. Neogrady, T. B. Pedersen, M. Pitonak, M. Reiher, B. O. Roos, L. Serrano-Andres, M. Urban, V. Veryazov and R. Lindh, *J. Comp. Chem.,* 2010, **31**, 224.

29 (a) K. Bernot, J. Luzon, L. Bogani, M. Etienne, C. Sangregorio, M. Shanmugam, A. Caneschi, R. Sessoli and D. Gatteschi, *J. Am. Chem. Soc.*, 2009, **131**, 5573; (b) G. Cucinotta, M. Perfetti, J. Luzón, M. Etienne, P.-E. Car, A. Caneschi, G. Calvez, K. Bernot and R. Sessoli, *Angew. Chem., Int. Ed.,* 2012, **51**, 1606.

30 A. Tanaka, J.W. Tucker and T. Idogaki, *J. Magn. Magn. Mat.,* 1996, **154**, 231.

31 (a) R. Navarro and L. J. de Jongh, *Physica B&C,* 1978, **94,** 67; (b) R. Navarro, *Magnetic properties of layered transition metal compounds, Physics and Chemistry of Materials with low dimensional structures*, Springer 1990, **9**, 105.

32 L.J. de Jongh and A.R. Miedema, *in Experimemts on simple magnetic model systems*, Advances in Physics 1974, 1, 1.

33 F. Luis, M.J. Martínez-Pérez, O. Montero, E. Coronado, S. Cardona-Sertra, C. Martí-Gastaldo, J.M. Clemente-Juan, J. Sesé, D. Drung and T. Schurig, *Phys. Rev. B*, 2010, **82**, 060403(R).

34 (a) N.V. Prokof'ev and P.C.E. Stamp, *Phys. Rev. Lett*., 1988, **80**, 5794; (b) W. Wernsdörfer, T. Ohm, C. Sangregorio, R. Sessoli, D. Mailly and C. Paulsen, *Phys. Rev. Lett*., 1999, **82**, 3903.

35 J. Bartolomé, J.A. Rojo, R. Navarro, D. González, M.R. Ibarra and A. del Moral, *J. Mag. Magn. Mat*., 1983, **31**, 1052.

36 X. –T. Liu, X. –Y. Wang, W. –X. Zhang, P. Cui and S. Gao, *Adv. Mater.,* **2006**, *18*, 2852.

37 M. Balanda, *Act. Phys. Pol. A*, 2013, **124**, 6.

38 Y-Z. Zheng, W. Xue, M.-L. Tong, X.-M. Chen, F. Grandjean and G. J. Long, *Inorg. Chem.*, 2008, **47**, 4077.

39 P.C. Hohenberg and B.I. Halperin, *Rev. Mod. Phys*., 1977, **49**, 435.

40 E. Stryjewski and N. Giordano, *Adv. in Phys*., 1977, **26**, 487.

41 M. Jeletic, P.-H. Lin, J. J. Le Roy, I. Korobkov, S. I. Gorelsky and M. Murugesu, *J. Am. Chem. Soc.*, 2011, **133**, 19286.

42 P.-E. Car, M. Perfetti, M. Mannini, A. Favre, A. Caneschi and R. Sessoli, *Chem. Commun*., 2011, **47**, 3751.

43 B. Liu, B-W. Wang, Z-M. Wang and S. Gao, *Sci. China, Chem.,* 2012, **5**, 926.

44 (a) M. Orendáč, L. Sedláková, E. Čižmár, A. Orendáčová, and A. Feher, S. A. Zvyagin and J. Wosnitza, W. H. Zhu, Z. M. Wang and S. Gao, *Phys. Rev. B*, 2010, **81**, 214410; (b) R. Schenker, M. N. Leuenberger, G. Chaboussant, D. Loss and H. U. Güdel, *Phys. Rev. B*, 2005, **72**, 184403.

45 D. L. Huber, *Phys. Rev. B*, 1965, **139**, A1684.

46 (a) D. M. Evans, A.Schilling, A. Kumar, D. Sanchez, N. Ortega, M. Arredonde, R. S. Kativar, J. M. Gregg and J. F. Scott, *Nature*, 2013, **4**, 1534; (b) A. Sawa, *Mat. Today*, 2008, **11**, 28.

47 P. Panissod and M. Drillon, in *Magnetism: Molecules to Materials IV*. Edited by Joel S. Miller and Marc Drillon, 2002 Wiley-VCH Verlag GmbH & Co. KgaA.

48 M. Evangelisti, F. Luis, F. L. Mettes, N. Aliaga, G. Aromí, J. J. Alonso, G. Christou and L. J. de Jongh, *Phys. Rev. Lett.* 2004, **93**, 117202.

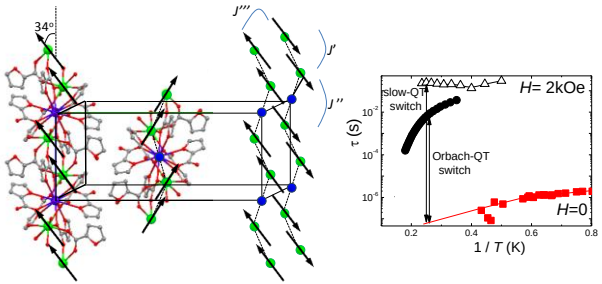

The new complex $\{Dy_2Ba(\alpha\text{-fur})_8\}_n$ has been synthesized, structurally characterized, and magnetically investigated down to 85 mK, allowing us to observe field induced slow relaxation behavior and 3D long-range ordering at T_N=0.25K.